THE WINDS OF SOLAR-LIKE MAIN SEQUENCE STARS

B. E. Wood[1], S. Redfield[2], J. L. Linsky[1], H. -R. Müller[3,4], and G. P. Zank[4]

[1]JILA, University of Colorado and NIST, Boulder, CO 80309-0440
[2]McDonald Observatory, University of Texas, Austin, TX 78712-0259
[3]Department of Physics and Astronomy, Dartmouth College, 6127 Wilder Lab, Hanover, NH 03755-3528
[4]Institute of Geophysics and Planetary Physics, University of California at Riverside, 1432 Geology, Riverside, CA 92521

Abstract

We have recently completed a survey of archival Lyα spectra of cool main sequence stars within 100 pc using data from the Hubble Space Telescope. The H I Lyα absorption lines were analyzed in part to measure properties of the interstellar medium along the observed lines of sight, but the primary goal was to search for evidence of H I absorption from the outer heliosphere and from the analogous astrospheres surrounding the observed stars. The astrospheric absorption is of particular interest because it provides the first method by which one can detect the coronal winds of solar-like stars. We report here 7 new detections of astrospheric absorption, although 2 are marginal, and 4 new detections of heliospheric absorption. This roughly doubles the number of previous astrospheric and heliospheric absorption detections. We report the results of preliminary efforts to use the astrospheric detections to measure mass loss rates for the observed cool stars, and we make some preliminary inferences on what these measurements imply for how mass loss relates to age and activity for solar-like stars.

Key words: stellar winds — ultraviolet spectra — heliosphere — Hubble Space Telescope — interstellar medium — solar wind

1. Introduction

One of the more recent solar phenomena to finally be detected for solar-like stars is the solar wind. Coronal winds like that of the Sun simply are not very easy to detect. The solar wind itself is not easy to detect from Earth despite the fact that we are basically living inside it. Almost everything we know about the solar wind comes from satellites that travel through it and measure its properties, but obviously we cannot study *stellar* winds like this. However, solar-like stellar winds can be detected indirectly by detecting the interaction regions produced by the collisions between the winds and the interstellar medium (ISM). These interaction regions are called "astrospheres," analogous to the heliosphere around the Sun, the large scale structure of which is defined by the solar wind's interaction with the ISM.

Detecting astrospheres requires spectra of stellar H I Lyα lines at 1215.67 Å with sufficient spectral resolution to resolve the neutral deuterium (D I) and hydrogen (H I) absorption profiles that are invariably superimposed on the stellar emission lines. The D I absorption is entirely from the ISM, and much of the H I absorption is as well, so the D I+H I Lyα absorption lines have frequently been used in the past to study the properties of the local ISM. However, for lines of sight where the ISM H I column density is sufficiently low and the ISM H I absorption sufficiently narrow, H I absorption from hot hydrogen in the outer heliosphere and from the astrospheres of the observed stars can also sometimes be discerned (Linsky & Wood 1996; Wood et al. 1996; Izmodenov et al. 1999; Wood & Linsky 1998).

The heliospheric absorption provides unique diagnostics for a part of the heliosphere that is otherwise completely undetectable. The astrospheric absorption has been used to provide the first mass loss measurements for solar-like stars, allowing the first studies to be made of the dependence of mass loss on age and activity for cool main sequence stars. However, the total number of heliospheric and astrospheric detections is still very small. In this paper, we describe an attempt to use archival spectra from the Hubble Space Telescope (HST) to significantly increase the number of detections.

2. The HST Lyα Observations

The only instruments with the UV access and spectral resolution necessary to detect the heliospheric and astrospheric Lyα absorption are the UV spectrometers that have operated on board HST, first the Goddard High Resolution Spectrograph (GHRS), and then the Space Telescope Imaging Spectrograph (STIS) that replaced GHRS in 1997. However, with the apparent recent demise of STIS in 2004 August, even HST is no longer capable of making these observations. The Cosmic Origins Spectrograph (COS), which is a UV spectrometer that was originally intended for installation on HST but whose future is now uncertain, will not have sufficient spectral resolution for our purposes even if COS does eventually find its way into orbit. Thus, the existing Lyα spectra that have already been obtained by GHRS and STIS will for the foreseeable future provide the only relevant data that can be used to study solar-like stellar winds.

In the top section of Table 1, we list 19 lines of sight with high resolution HST Lyα spectra that have already been analyzed and published (Bertin et al. 1995; Linsky et al. 1995; Linsky & Wood 1996; Wood et al. 1996; Dring et al. 1997; Piskunov et al. 1997; Wood & Linsky 1998; Wood et al. 2000a; Wood et al. 2001; Kruk et al. 2002; Lemoine et al. 2002). All these data are GHRS spectra except for 36 Oph, which is STIS. The seventh column of Table 1 lists the ISM H I column densities (in cm^{-2}) measured towards the observed stars. The eighth column indicates whether high resolution HST spectra of the interstellar Mg II h & k absorption lines (at 2803 Å and 2796 Å, respectively) are available to provide information on the velocity structure of the ISM. When available, this information is always taken into account in the analysis of the broad, saturated ISM H I Lyα absorption (see below).

The ninth and tenth columns of Table 1 indicate which Lyα spectra show the presence of heliospheric absorption and astrospheric absorption, respectively, in addition to the ISM absorption. Marginal detections are indicated by question marks after the "Yes." Whether a detection is marginal or not is based on our own determination, after inspecting and working with the data ourselves. Lemoine et al. (2002) and Vidal-Madjar & Ferlet (2002) claim to see evidence for weak heliospheric absorption towards the similar Capella and G191-B2B lines of sight, but these claims rely on subtle statistical arguments rather than clearly visible excess absorption, so we do not consider these to be detections for our purposes here. As indicated by the top portion of Table 1, there are currently only 6 astrospheric detections and 4 heliospheric detections, if one considers the Alpha/Proxima Cen observations as a single line of sight.

However, there are many archival HST Lyα spectra that have not yet been analyzed. We have searched the HST archives for UV spectroscopic observations of cool stars that could potentially provide new detections of heliospheric and astrospheric absorption. The ISM H I absorption would almost certainly be too strong to hope to detect heliospheric and astrospheric absorption for very distant targets, so we confine our attention to lines of sight shorter than 100 pc. We find 33 previously unanalyzed spectra to analyze. These lines of sight are listed in the bottom portion of Table 1. The previously unanalyzed data are all STIS spectra taken with the moderate resolution E140M grating. For a precise analysis, we require that the D I absorption profile be at least mostly resolved, and with a resolution of $\lambda/\Delta\lambda \approx 45,000$, E140M spectra just barely have sufficient spectral resolution for our purposes.

3. Data Analysis

Figure 1 shows an example of one of the 33 previously unanalyzed Lyα spectra. The spectrum is typical in showing a very broad, saturated H I absorption line, and a much narrower D I absorption line -0.33 Å from the center of the H I line. A full description of how the Lyα absorption lines are analyzed will be provided elsewhere (Wood et al. 2004, in preparation), but we provide here a brief description of the process.

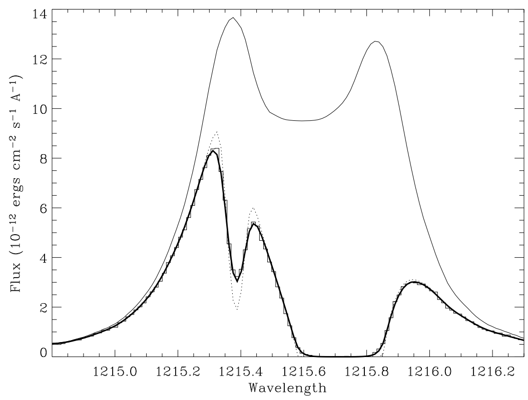

Figure 1. HST/STIS E140M spectrum of the Lyα line of τ Ceti, showing broad ISM H I absorption and narrow ISM D I absorption -0.33 Å from the center of the H I line. The thin solid line is the reconstructed stellar emission line profile. The dotted and thick solid lines are fits to the ISM absorption before and after convolution with the instrumental LSF.

Since the D I absorption is narrow, optically thin, and will never be contaminated by heliospheric/astrospheric absorption, the D I line provides much more precise measurements for the ISM than the saturated H I absorption. Thus, in analyzing the H I lines, we fit the D I and H I Lyα absorption simultaneously, in order to allow the D I absorption to constrain the ISM H I absorption. In particular, we force the D I and H I centroid velocities to be the same, and we force their Doppler parameters to be consistent with $b(\mathrm{H\ I}) = \sqrt{2}b(\mathrm{H\ I})$, which is a good approximation since the D I and H I lines are known to be dominated by thermal broadening. Finally, since recent work has demonstrated that the D/H ratio is constant in the local ISM, we simply assume that $\mathrm{D/H} = 1.5 \times 10^{-5}$ for all our lines of sight, which is consistent with several recent determinations (Linsky 1998; Moos et al. 2002; Wood et al. 2004).

For the lines of sight that have information on the ISM velocity structure from high resolution Mg II spectra (see Table 1), we take this information into account in our fits, performing multi-component fits when the Mg II absorption suggests the presence of multiple components. Redfield & Linsky (2002) have already analyzed the Mg II absorption lines, so in cases where multiple ISM components are present we use their measurements to tell us what the velocity separations and column density ratios should be for the individual components.

Table 1. Line of sight information for HST Lyα targets.

HD #	Other Name	Spectral Type	Dist. (pc)	l (deg)	b (deg)	log N(H I)	Mg II?	Hel. Det.?	Ast. Det.?
				PREVIOUS ANALYSES					
	Proxima Cen	M5.5 V	1.30	313.9	-1.9	17.61	No	Yes	No
128620	α Cen A	G2 V	1.35	315.7	-0.7	17.61	Yes	Yes	Yes
128621	α Cen B	K0 V	1.35	315.7	-0.7	17.61	Yes	Yes	Yes
48915	Sirius	A1 V	2.64	227.2	-8.9	17.53	Yes	Yes	...
22049	ϵ Eri	K1 V	3.22	195.8	-48.1	17.88	Yes	No	Yes
201091	61 Cyg A	K5 V	3.48	82.3	-5.8	18.13	Yes	No	Yes
209100	ϵ Ind	K5 V	3.63	336.2	-48.0	18.00	No	No	Yes
26965	40 Eri A	K1 V	5.04	200.8	-38.1	17.85	Yes	No	No
155886	36 Oph A	K1 V	5.99	358.3	6.9	17.85	Yes	Yes	Yes
62509	β Gem	K0 III	10.3	192.2	23.4	18.26	Yes	No	No
34029	Capella	G8 III+G1 III	12.9	162.6	4.6	18.24	Yes	No	No
432	β Cas	F2 IV	16.7	117.5	-3.3	18.13	Yes	No	No
11443	α Tri	F6 IV	19.7	138.6	-31.4	18.33	Yes	No	No
222107	λ And	G8 IV-III+M V	25.8	109.9	-14.5	18.45	No	No	Yes?
22468	HR 1099	K1 IV+G5 IV	29.0	184.9	-41.6	18.13	Yes	No	No
	HZ 43	DA	32.0	54.1	84.2	17.93	Yes	Yes?	...
62044	σ Gem	K1 III	37.5	191.2	23.3	18.20	Yes	No	No
	G191-B2B	DA	68.8	156.0	7.1	18.18	Yes	No	...
111812	31 Com	G0 III	94.2	115.0	89.6	17.88	Yes	No	No
				NEW ANALYSES					
10700	τ Cet	G8 V	3.65	173.1	-73.4	18.01	No	No	No
	AD Leo	M3.5 V	4.69	216.5	54.6	18.47	No	No	No
	EV Lac	M3.5 V	5.05	100.6	-13.1	17.97	No	No	Yes
165341	70 Oph A	K0 V	5.09	29.9	11.4	18.06	Yes	Yes	Yes
131156A	ξ Boo A	G8 V	6.70	23.1	61.4	17.92	Yes	Yes	Yes
115617	61 Vir	G5 V	8.53	311.9	44.1	17.91	No	Yes	Yes?
39587	χ^1 Ori	G0 V	8.66	188.5	-2.7	17.93	Yes	No	No
23249	δ Eri	K0 IV	9.04	198.1	-46.0	17.88	No	No	Yes
20630	κ Cet	G5 V	9.16	178.2	-43.1	17.89	Yes	No	No
197481	AU Mic	M0 V	9.94	12.7	-36.8	18.36	Yes	No	No
33262	ζ Dor	F7 V	11.7	266.0	-36.7	18.29	Yes	No	No
37394	HR 1925	K1 V	12.2	158.4	12.0	18.26	No	No	No
166	HR 8	K0 V	13.7	111.3	-32.8	18.29	No	No	No
142373	χ Her	F8 V	15.9	67.7	50.3	18.25	No	No	No
43162	HR 2225	G5 V	16.7	230.9	-18.5	17.87	No	No	No
165185	HR 6748	G5 V	17.4	356.0	-7.3	18.13	No	Yes	No
203244	SAO 254993	G5 V	20.5	324.9	-38.9	18.82	No	No	No
97334	HR 4345	G0 V	21.7	184.3	67.3	17.82	No	No	No
59967	HR 2882	G4 V	21.8	250.5	-9.0	18.54	No	No	No
116956	SAO 28753	G9 IV-V	21.9	113.7	59.5	18.19	No	No	No
106516	HR 4657	F5 V	22.6	288.5	51.5	18.57	No	No	No
73350	SAO 136111	G0 V	23.6	232.1	20.0	18.16	No	No	No
128987	SAO 158720	G6 V	23.6	337.5	39.2	18.11	No	No	Yes
82210	DK UMa	G4 III-IV	32.4	142.6	38.9	18.05	Yes	No	Yes?
93497	μ Vel	G5 III	35.3	283.0	8.6	18.47	No	No	No
28568	SAO 93981	F2 V	41.2	180.5	-21.4	18.12	Yes	No	No
28205	V993 Tau	G0 V	45.8	180.4	-22.4	18.11	Yes	No	No
28033	SAO 76609	F8 V	46.4	175.4	-18.9	18.15	Yes	No	No
	V471 Tau	K0 V	46.8	172.5	-27.9	18.21	No	No	No
209458	V376 Peg	G0 V	47.1	76.8	-28.5	18.37	No	No	No
220657	υ Peg	F8 III	53.1	98.6	-35.4	18.24	Yes	No	No
32008	HR 1608	G7 IV-III	54.7	209.6	-29.4	18.08	No	No	No
203387	ι Cap	G8 III	66.1	33.6	-40.8	18.70	Yes	No	No

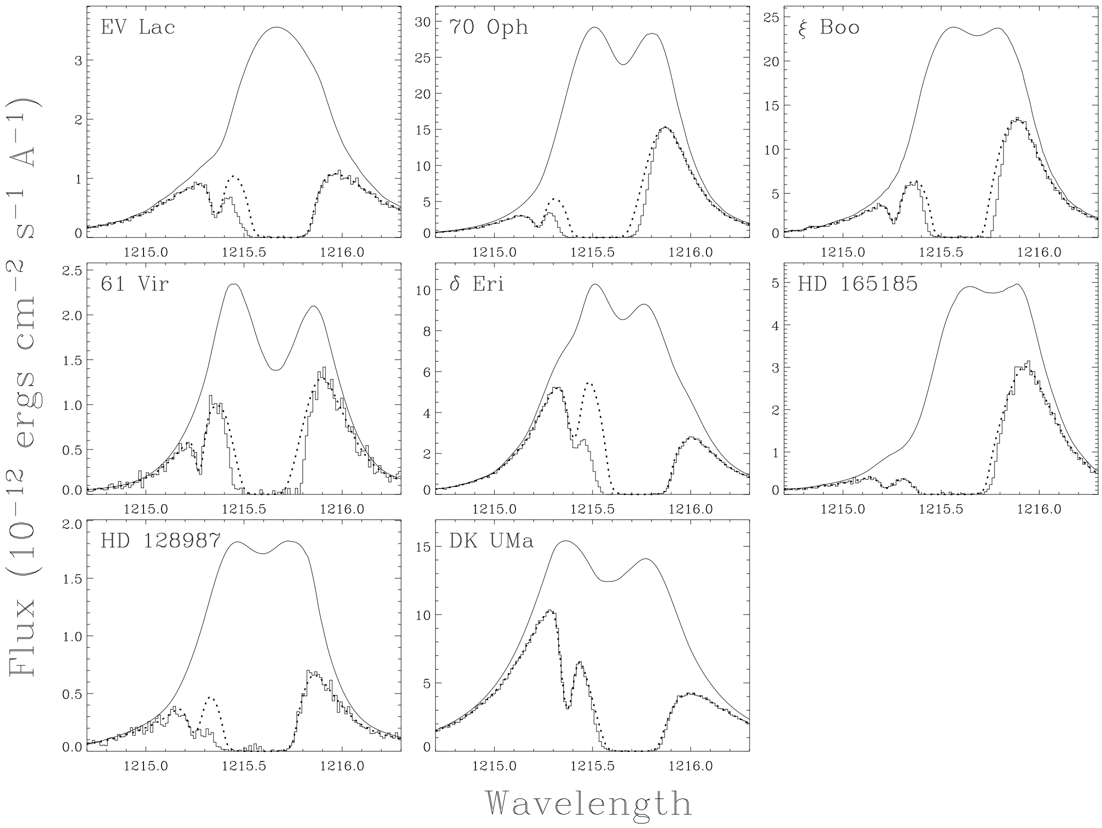

Figure 2. The Lyα absorption spectra that we are unable to fit with only ISM absorption. The dotted line shows the absorption from the ISM. The excess absorption seen on the red side of the absorptionline for some of these stars is from the heliosphere and the blue-side excess absorption, when present, is astrospheric.

Analyzing the Lyα absorption requires the reconstruction of the stellar Lyα profile. For each Lyα spectrum, an initial estimate is made of the intrinsic stellar Lyα profile overlying the absorption. After an initial fit is made, the residuals of the fit are used to alter the assumed stellar profile. A second fit is then performed, which should be better than the first. Additional iterations refine the fit and the assumed stellar profile even further. This iterative process ultimately leads to our final, best fit to the data, such as the fit to the τ Ceti Lyα line shown in Figure 1.

For 25 of the 33 new Lyα spectra, we are able to successfully fit the data with only ISM absorption. Figure 1 shows an example of one of these fits. However, for 8 of the 33 lines of sight it is not possible to fit D I and H I in a self-consistent manner without including an H I absorption component that contributes no absorption to D I. Figure 2 shows these 8 Lyα spectra and shows the H I+D I absorption that we believe is coming only from the ISM. The discrepancy with the data indicates the excess H I absorption that we believe is heliospheric and/or astrospheric absorption.

Theoretical models have shown that the heliosphere only produces excess absorption on the red side of the Lyα absorption line, while astrospheric absorption produces excess absorption on the blue side of the line (Gayley et al. 1997; Izmodenov et al. 1999; Wood et al. 2000b). The redshift of heliospheric absorption relative to the ISM is mostly due to the deceleration and deflection of H atoms as they cross the bow shock, where the corresponding effect for astrospheres results instead in a blueshift since our perspective is from outside the astrosphere rather than inside. Thus, Figure 2 suggests that we have detected seven new astrospheres (EV Lac, 70 Oph, ξ Boo, 61 Vir, δ Eri, HD 128987, and DK UMa), and we have four new heliospheric absorption detections (70 Oph, ξ Boo, 61 Vir, and HD 165185). These results are summarized in the last 2 columns in Table 1. Note that we consider the 61 Vir and DK UMa astrospheric detections to be marginal ones.

4. The Heliospheric Absorption

Our four new heliospheric detections bring the total number of detections up to eight, if one counts the α Cen and

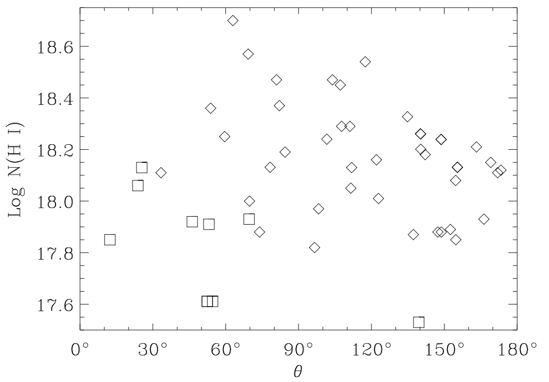

Figure 3. The ISM H I column densities measured for all HST-observed lines of sight are plotted versus the angle of the lines of sight relative to the upwind direction of the ISM flow seen by the Sun. The boxes and diamonds indicate lines of sight that yield detections and nondetections of heliospheric absorption, respectively.

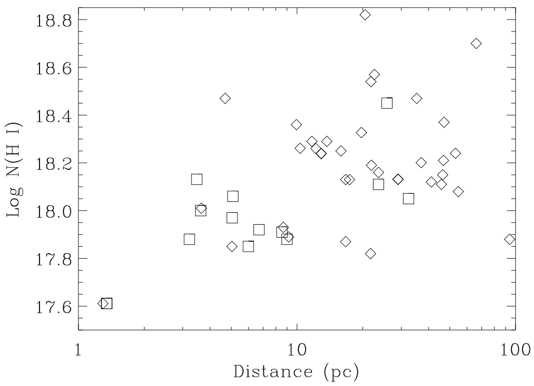

Figure 4. The ISM H I column densities measured for all HST-observed lines of sight are plotted versus distance. The boxes and diamonds indicate lines of sight that yield detections and nondetections of astrospheric absorption, respectively.

Proxima Cen detections as a single detection. There are now a sufficient number of detections to investigate what distiguishes the lines of sight that yield heliospheric detections from the majority that do not. In Figure 3, we plot the ISM H I column density measured for all HST-observed lines of sight versus the angle of the line of sight with respect to the upwind direction of the ISM flow seen by the Sun. The boxes in the figure indicate the sight lines that yield heliospheric detections and the diamonds indicate lines of sight that show no evidence for heliospheric absorption.

The detections and nondetections are nicely separated in Figure 3. The detections tend to be for lines of sight with low ISM H I column densities. This makes sense, since the ISM absorption will be broader for higher column densities, which will hide the heliospheric absorption for sufficiently high H I columns. Figure 3 also shows that it is much easier to detect heliospheric absorption in upwind directions than in downwind directions. For $\theta < 60°$, the ISM column density has to be $\log N(\mathrm{H\ I}) < 18.2$ to allow the detection of heliospheric absorption, while in downwind directions one must have $\log N(\mathrm{H\ I}) < 17.8$. This behavior is also understandable, since it is in upwind directions where the deceleration of the ISM H I gas due to its interaction with the solar wind is strongest, which shifts the heliospheric absorption away from the ISM absorption to a greater extent, making it easier to detect. Note that these results represent another strong argument in favor of heliospheric absorption being the correct interpretation for the redshifted excess H I Lyα absorption.

The θ value in Figure 3 is sufficient to fully describe a line of sight through the heliosphere only if the heliosphere is precisely axisymmetric. However, there could be significant deviations in axisymmetry due to latitudinal solar wind variations, an ISM magnetic field that is skewed with respect to the ISM flow direction, or unstable MHD phenomena near the plane of the heliospheric current sheet (Pauls & Zank 1997; Ratkiewicz et al. 1998; Opher et al. 2003). With eight detections of absorption from the outer heliosphere, we can begin to look for evidence for any of these asymmetries, which will be a project for the near future.

5. The Astrospheric Absorption

Our new astrospheric detections have increased the total number of detections from 6 to 13 (see Table 1). In Figure 4 we plot the ISM H I column densities for the HST-observed lines of sight versus distance, and we use boxes and diamonds to distinguish between spectra that show astrospheric absorption and those that do not. Within 10 pc the detection percentage is very high, $\sim 60\%$, but this percentage falls below 10% outside 10 pc. The principle reason for this distance dependence is the general increase in $N(\mathrm{H\ I})$ with distance, which makes it harder to detect astrospheric absorption just as it makes it harder to detect heliospheric absorption (see Fig. 3).

However, a contributing factor in the difficulty in finding astrospheric detections beyond 10 pc is that many of these stars will be surrounded by completely ionized ISM material that will inject no H I atoms into the astrospheres for us to detect. The Sun is located in a region of space called the Local Bubble in which much of the volume of the Bubble is filled with hot, ionized material, which is believed to be responsible for most of the soft X-ray background radiation. However, there are warm, partially neutral clouds within the Local Bubble, and the Sun happens to be within one of these. Very nearby stars within 10 pc

Table 2. Mass loss measurements from astrospheric absorption detections.

Star	Spectral Type	d (pc)	V_{ISM} (km s^{-1})	θ (deg)	$\dot{M}$ ($\dot{M}_\odot$)	Log L$_x$	Surf. Area (A$_\odot$)
α Cen	G2 V+K0 V	1.3	25	79	2	27.34	2.37
Proxima Cen	M5.5 V	1.3	25	79	<0.2	27.23	0.026
ϵ Eri	K1 V	3.2	27	76	30	28.32	0.62
61 Cyg A	K5 V	3.5	86	46	0.5	27.26	0.45
ϵ Ind	K5 V	3.6	68	64	0.5	27.18	0.50
EV Lac	M3.5 V	5.1	45	84	1	28.76	0.096
70 Oph	K0 V+K5 V	5.1	37	120	100	28.45	1.32
36 Oph	K1 V+K1 V	5.5	40	134	15	28.28	0.88
ξ Boo	G8 V+K4 V	6.7	32	131	5	28.94	1.00
61 Vir	G5 V	8.5	51	98	0.3	26.93	1.10
δ Eri	K0 IV	9.0	37	41	?	27.05	6.66
HD 128987	G6 V	24	8	79	?	28.65	0.76
λ And	G8 IV-III+M V	26	53	89	5	30.48	55
DK UMa	G4 III-IV	32	43	32	0.15	30.34	19.4

will be more likely to also be within the same warm cloud than more distant targets.

The primary use of the astrospheric absorption is as a diagnostic of the stellar wind. A stronger wind will produce a larger astrosphere with larger astrospheric H I column densities and therefore more Lyα absorption. Thus, the astrospheric absorption can be used to estimate mass loss rates for the stars with detected absorption. Mass loss rates have already been estimated for the old astrospheric detections (Müller et al. 2001a,b; Wood et al. 2001; Wood et al. 2002). We are still in the process of making analogous measurements for the new astrospheric detections reported here, but we can report some preliminary results of this analysis.

Table 2 lists all the astrospheric detections and resulting mass loss measurements, both old and new. The table lists the spectral types of the stars, where for binary stars there is often more than one star within the same astrosphere, meaning the measured mass loss rate will be indicative of the combined mass loss of both stars. In those cases, the stellar surface areas in Table 2 are the combined surface areas of both stars. The V_{ISM} values in Table 2 indicate the ISM velocity seen by each star, and θ is the angle between the observed line of sight and the upwind direction of the ISM flow seen by the star. These quantities, which can be computed from the local ISM flow vector and the known proper motions of these nearby stars, must be known to infer mass loss rates from the astrospheric absorption (see below).

We refer the reader to Wood et al. (2002) for a detailed discussion of the mass loss measurement process, but we summarize the method here. Extracting mass loss rates from the astrospheric absorption requires the assistance of hydrodynamic models of the astrospheres, analogous to heliospheric models that have been successful in reproducing the heliospheric absorption (Wood et al. 2000b; Izmodenov et al. 2002). Our astrospheric models are extrapolated from a four-fluid heliospheric model of a type described by Zank et al. (1996) that Wood et al. (2000b) demonstrated fitted the heliospheric data. In converting this heliospheric model to an astrospheric model, we change the V_{ISM} value to the value appropriate for the star (see Table 2), we change the assumed stellar wind density to a value appropriate for the mass loss rate we wish to assume, and we then recompute the model. From the model, we can estimate astrospheric H I Lyα absorption for the observed line of sight, as defined by the θ value in Table 2. This absorption is compared with the data and the mass loss rate is modified until agreement with the data is achieved.

We have so far computed enough astrospheric models to obtain good mass loss rate estimates for five of our new astrospheric detections, and in Figure 5 the Lyα absorption profiles of these lines of sight are compared with the predictions of the best-fit models. Mass loss rates are quoted relative to the solar value of $\dot{M}_\odot \approx 2 \times 10^{-14}$ $M_\odot$ yr^{-1}. The new mass loss measurements range from a very low value of $\dot{M} = 0.15\dot{M}_\odot$ for DK UMa, which is the lowest mass loss rate yet measured for a star of any kind, up to $\dot{M} = 100\dot{M}_\odot$ for 70 Oph, which is the strongest coronal wind yet measured. It should be noted that when evaluating how well a model fits the data, it is more important that the model fits the data well near the base of the H I absorption than elsewhere. Discrepancies farther from the core of the absorption can often be resolved by altering the assumed stellar emission profile, but discrepancies near the base of the absorption are much harder to fix. Thus, the $\dot{M} = 1\dot{M}_\odot$ model for EV Lac in Figure 5, for example, is a better fit than it might appear at first glance.

The mass loss measurements are summarized in Table 2. We do not yet have any estimate for δ Eri and HD 128987. It is worth mentioning that the astrospheric detection for HD 128987 is surprising considering the very

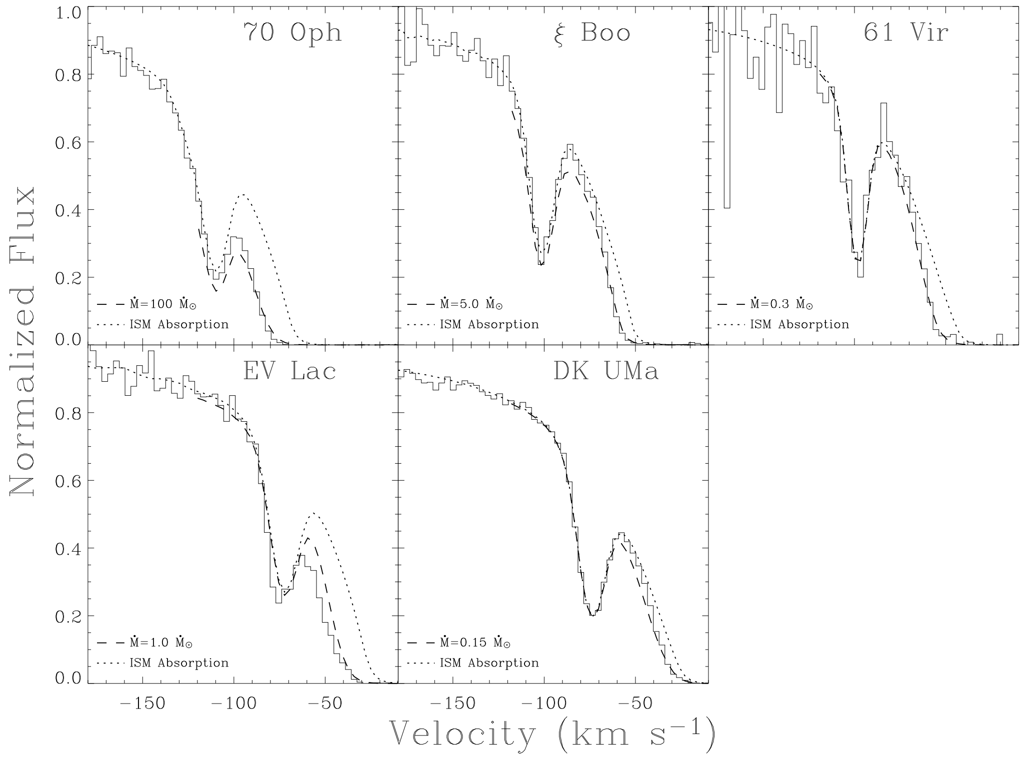

Figure 5. The blue side of the H I Lyα absorption lines for five of the stars with detected astrospheric absorption. The dotted lines show the ISM absorption alone. The dashed lines show the additional astrospheric absorption predicted by models assuming various mass loss rates. Only the models that best fit the data are shown.

low $V_{ISM} = 8$ km s^{-1} velocity for this star (see Table 2). The larger the ISM wind speed seen by a star, the more heating there is at the stellar bow shock, and therefore the hotter the astrospheric H I. Hotter H I produces broader and easier to detect Lyα absorption. Thus, conventional wisdom suggests that stars with detected astrospheres should tend to have high V_{ISM} values, and indeed inspection of Table 2 shows that all the other detections have V_{ISM} comparable to or higher than the solar value of $V_{ISM} = 26$ km s^{-1}. The ISM velocity seen by HD 128987 is so slow that there will not even be a stellar bow shock for this star, so we anticipate that models may have difficulty explaining this astrospheric detection.

6. Mass Loss Versus Activity

The winds of solar-like stars originate in their hot coronae, so it is natural to wonder if the stellar mass loss rates are correlated with coronal properties. Stellar coronae are prodigious sources of X-rays, so X-ray emission is a widely available diagnostic for coronal activity. Thus, in Table 2 we list X-ray luminosities for the stars with astrospheric detections, and in Figure 6 we plot the mass loss rates per unit surface area versus X-ray surface flux. Below $\log F_X < 8\times10^5$ ergs cm^{-2} s^{-1}, mass loss rates appear to increase with activity in a manner consistent with the power law relation that is fitted to the data, which is

$$\dot{M} \propto F_x^{1.30\pm0.17}. \qquad (1)$$

This mass-loss/activity corelation was first noted by Wood et al. (2002). Two of our new mass loss measurements (61 Vir and 70 Oph) are for stars in the low activity regime where this correlation applies. The two new data points support the existence of the mass-loss/activity correlation and do not change the inferred power law relation very much.

The situation is much more muddled at high activity levels of $\log F_X > 8\times10^5$ ergs cm^{-2} s^{-1}, where none of the five data points are consistent with the mass-loss/activity relation inferred from the lower activity stars. One problem is that the selection of stars in the high activity regime is very diverse. In the lower activity regime, all the measured stars are fairly solar-like G and K dwarf stars, but the high activity regime includes M dwarfs (Proxima Cen

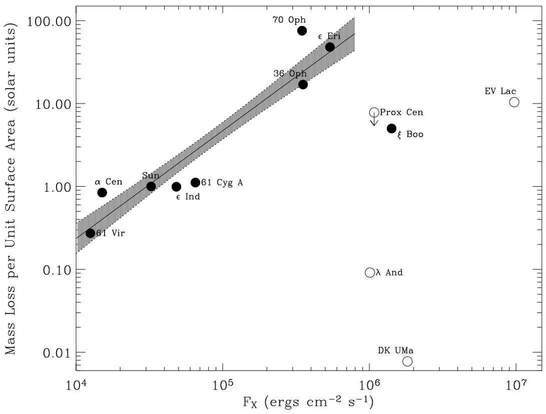

Figure 6. Mass loss rates per unit surface area plotted versus stellar X-ray surface fluxes. Filled symbols are for solar-like G and K dwarf stars, while open symbols are for less solar-like cool main-sequence stars. For stars with $\log F_X < 8\times10^5$ ergs cm^{-2} s^{-1}, mass loss increases with X-ray flux and we have fitted a power law to these data points. However, it is unclear what happens at higher activity levels.

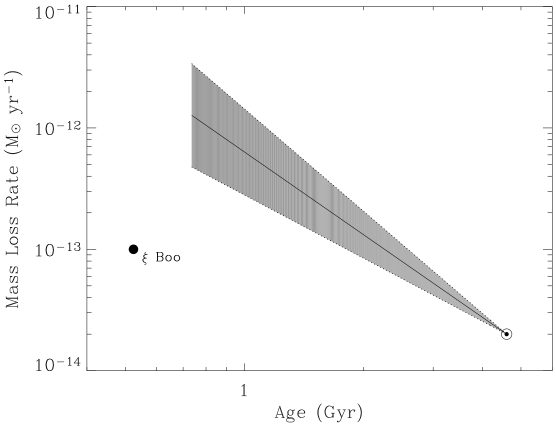

Figure 7. The mass loss history of the Sun inferred from the power law relation from Fig. 6. The truncation of the mass-loss/activity relation in Fig. 6 means the mass-loss/age relation is truncated as well. It is difficult to say what happens at earlier times, but the ξ Boo mass loss measurement shown in the figure suggests that not only does the power law increase in mass loss towards earlier times not continue, but the wind may suddenly get weaker at $t\approx0.7$ Gyr as one goes back in time.

and EV Lac) and evolved stars (DK UMa and λ And). Wood et al. (2002) had previously suggested that λ And and Proxima Cen were discrepant simply because they are not G and K dwarf stars. This argument might also work for the new measurements of EV Lac and DK UMa, but it should not work for ξ Boo, which is a binary system consisting of two relatively solar-like stars (G8 V+K4 V).

The ξ Boo data point in Figure 6 lies well below the power law relation along with the M dwarfs and evolved stars, which suggests that there really is a change in the nature of the relation between stellar winds and activity at $\log F_X\sim8\times10^5$ ergs cm^{-2} s^{-1}. Thus, the power law relation in Figure 6 is truncated at this location.

Unfortunately, the existing data do not clearly indicate what the mass-loss/activity relation becomes in the high activity regime, or even if there is any such relation. The two evolved stars (DK UMa and λ And) are very discrepant from the three dwarf stars (ξ Boo, Proxima Cen, and EV Lac), suggesting that activity and winds are not related in the same way for evolved stars and main sequence stars. The three dwarfs might have self-consistent mass loss measurements, but even if one considers the M dwarf and ξ Boo data points together, two mass loss measurements and one upper limit are too small a sample to clearly define what is happening to the dwarf star mass-loss/activity relation above $\log F_X = 8\times10^5$ ergs cm^{-2} s^{-1}. Thus, all that can be said at this point is that there is evidence that the mass-loss/activity relation changes at high activity levels, but it is not yet clear exactly what happens to it.

What might cause the mass-loss/activity relation to change at high activity levels? One possible explanation concerns the appearance of polar spots for very active stars. Low activity stars presumably have starspot patterns similar to that of the Sun, where all spots are confined to low latitudes. However, for very active stars not only are spots detected at high latitudes, but a majority of these stars show evidence for large polar spots (Strassmeier 2002). This represents a fundamental change in the stellar magnetic geometry, which has been investigated theoretically by Schrijver & Title (2001). It is quite plausible to suppose that this dramatic change in the magnetic field structure could affect the winds coming from these active stars. We hypothesize that stars with polar spots might have a magnetic field with a strong dipolar component that could envelope the entire star and inhibit stellar outflows, thereby explaining why active stars have weaker winds than the mass-loss/activity relation of less active stars would predict.

7. Mass Loss Versus Age

The mass-loss/activity relation in eqn. (1) can be combined with known relations between activity and age to derive an empirical mass loss evolution law for solar-like stars. From Ayres (1997), we find

$$F_x \propto t^{-1.74\pm0.34}. \quad (2)$$

Combining this with eqn. (1) yields

$$\dot{M} \propto t^{-2.26\pm0.53}. \quad (3)$$

Figure 7 shows what this relation suggests for the mass loss history of the Sun. The truncation of the power law relation in Figure 6 leads to the mass-loss/age relation in Figure 7 being truncated as well at about $t = 0.7$ Gyr.

It is difficult to be sure exactly what the solar wind was like at earlier times, but the evidence from Figure 6 suggests that mass loss rates are significantly lower than would be predicted by the mass-loss/activity relation defined by the less active stars. The ξ Boo measurement is particularly relevant since the stars in this binary are the most solar-like of those with measured mass loss rates in this high activity regime. Thus, the location of ξ Boo is shown on Figure 7 in order to estimate what the solar wind might have been like at times earlier than $t = 0.7$ Gyr, where from eqn. (2) and ξ Boo's X-ray luminosity in Table 2 we have estimated an age for ξ Boo of $t = 0.52$ Gyr.

The history of the solar wind is not only of interest to solar/stellar astronomers, but it is also important for those who study planets because of the effects that the solar wind may have had on the atmospheres of the planets in the distant past. Of particular interest is the history of the Martian atmosphere, which was once much thicker than it is now and was presumably thick enough to allow water to exist on the surface of the planet despite this being impossible today (Jakosky & Phillips 2001). Currently, one of the most likely explanations for the disappearance of most of the Martian atmosphere is that it was eroded by solar wind sputtering (Luhmann et al. 1992, Jakosky et al. 1994; Kass & Yung 1995; Lammer et al. 2003). This did not happen for the Earth because the Earth's strong magnetosphere protects our atmosphere from solar wind erosion, but Mars lost its global magnetic field at least 3.9 Gyr ago (Acuña et al. 1999).

It is interesting to note that the age when Mars is believed to have lost its magnetic field and presumably most of its atmosphere is also roughly the age when Figure 7 suggests that the solar wind strengthened by about a factor of 10 and entered the low activity regime where the power law relation in eqn. (3) applies. Perhaps this strengthening of the solar wind played a role in the dissipation of the Martian atmosphere. Whatever the case, the generally stronger wind of the young Sun implied by Figure 7 makes it more likely that solar wind erosion has been an important process for the history of planetary atmospheres in our solar system. This connection with planetary science represents one of the most interesting applications of the empirical wind evolution law made possible by the astrospheric Lyα absorption measurements.

Acknowledgements

Support for this work was provided by grant AR-09957 from the Space Telescope Science Institute, which is operated by AURA, Inc., under NASA contract NAS5-26555. The first author also acknowledges the assistance of an International Travel Grant from the American Astronomical Society and the National Science Foundation.

References

Acuña, M. H., et al. 1999, Science, 284, 790
Ayres, T. R. 1997, J. Geophys. Res., 102, 1641
Bertin, P., Vidal-Madjar, A., Lallement, R., Ferlet, R., & Lemoine, M. 1995, A&A, 302, 889
Dring, A. R., Linsky, J., Murthy, J., Henry, R. C., Moos, W., Vidal-Madjar, A., Audouze, J., & Landsman, W. 1997, ApJ, 488, 760
Gayley, K. G., Zank, G. P., Pauls, H. L., Frisch, P. C., & Welty, D. E. 1997, ApJ, 487, 259
Izmodenov, V. V., Lallement, R., & Malama, Y. G. 1999, A&A, 342, L13
Izmodenov, V. V., Wood, B. E., & Lallement, R. 2002, J. Geophys. Res., 107, 1308
Jakosky, B. M., Pepin, R. O., Johnson, R. E., & Fox, J. L. 1994, Icarus, 111, 271
Jakosky, B. M., & Phillips, R. J. 2001, Nature, 412, 237
Kass, D. M., & Yung, Y. L. 1995, Science, 268, 697
Kruk, J. W., et al. 2002, ApJS, 140, 19
Lammer, H., Lichtenegger, H. I. M., Kolb, C., Ribas, I., Guinan, E. F., Abart, R., & Bauer, S. J. 2003, Icarus, 165, 9
Lemoine, M., et al. 2002, ApJS, 140, 67
Linsky, J. L. 1998, Space Sci. Rev., 84, 285
Linsky, J. L., Diplas, A., Wood, B. E., Brown, A., Ayres, T. R., & Savage, B. D. 1995, ApJ, 451, 335
Linsky, J. L., & Wood, B. E. 1996, ApJ, 463, 254
Moos, H. W., et al. 2002, ApJS, 140, 3
Müller, H. -R., Zank, G. P., & Wood, B. E. 2001a, ApJ, 551, 495
Müller, H. -R., Zank, G. P., & Wood, B. E. 2001b, in The Outer Heliosphere: The Next Frontiers, ed. K. Scherer et al. (Amsterdam: Pergamon), 53
Opher, M., Liewer, P. C., Gombosi, T. I., Manchester, W., DeZeeuw, D. L., Sokolov, I., & Toth, G. 2003, ApJ, 591, L61
Pauls, H. L. and Zank, G. P. 1997, J. Geophys. Res., 102, 19,779
Piskunov, N., Wood, B. E., Linsky, J. L., Dempsey, R. C., & Ayres, T. R. 1997, ApJ, 474, 315
Ratkiewicz, R., Barnes, A., Molvik, G. A., Spreiter, J. R., Stahara, S. S., Vinokur, M., & Venkateswaran, S. 1998, A&A, 335, 363
Redfield, S., & Linsky, J. L. 2002, ApJS, 139, 439
Schrijver, C. J., & Title, A. M. 2001, ApJ, 551, 1099
Strassmeier, K. G. 2002, Astronomische Nachrichten, 323, 309
Vidal-Madjar, A., & Ferlet, R. 2002, ApJ, 571, L169
Wood, B. E., Alexander, W. R., & Linsky, J. L. 1996, ApJ, 470, 1157
Wood, B. E., & Linsky, J. L. 1998, ApJ, 492, 788
Wood, B. E., Linsky, J.L., Hébrard, G., Williger, G. M., Moos, H. W., & Blair, W. P. 2004, ApJ, 609, 838.
Wood, B. E., Linsky, J. L., Müller, H. -R., & Zank, G. P. 2001, ApJ, 547, L49
Wood, B. E., Linsky, J. L., & Zank, G. P. 2000a, ApJ, 537, 304
Wood, B. E., Müller, H. -R., & Zank, G. P. 2000b, ApJ, 542, 493
Wood, B. E., Müller, H. -R., Zank, G. P., & Linsky, J. L. 2002, ApJ, 574, 412
Zank, G. P., Pauls, H. L., Williams, L. L., & Hall, D. T. 1996, J. Geophys. Res., 101, 21639